# Chapter 1
# Low-Modulus Ti Alloys Suitable for Rods in Spinal Fixation Devices

**Mitsuo Niinomi**

**Abstract** Low-Young's modulus Ti alloys are expected to be suitable for use in the rods of spinal fixation devices. However, in addition to a low Young's modulus, the rods must also exhibit a high Young's modulus at the deformed region to reduce springback when surgeons bend the rod inside the narrow bodies of patients. Ti–Mo and Ti–Cr alloys are potential candidates to satisfy these two conflicting demands. In these alloys, known as Young's modulus changeable or Young's modulus self-adjustable Ti alloys, the ω-phase with high Young's modulus is induced by deformation. Among these alloys, Ti–12Cr is judged to be the most suitable for use in the rods of spinal fixation devices. This alloy exhibits a high uniaxial fatigue strength, and its compressive fatigue strength is significantly improved by cavitation peening.

**Keywords** Low Young's modulus • Young's modulus self-adjustability • Ti–Cr alloy • Ti–Mo alloy • Spinal fixation device • Compressive fatigue strength • Cavitation peening

## 1.1 Introduction

To inhibit stress shielding, which is caused by the mismatch in Young's modulus between an implant and bone and leads to bone absorption and poor bone remodeling, low-Young's modulus titanium (Ti) alloys have been or are being developed for implant devices such as artificial hip joints, bone plates, and spinal fixation devices.

M. Niinomi (✉)
Institute for Materials Research, Tohoku University,
2-1-1 Katahira, Aoba-ku, Sendai, Miyagi 980-8577, Japan

Graduate School of Science and Technology, Meijyo University,
1-501, Shiogamaguchi, Tempaku-ku, Nagoya, Aichi 468-8502, Japan

Graduate School of Engineering, Osaka University, 2-1, Yamadagaoka,
Suita, Osaka 565-0871, Japan

Institute of Materials and Systems for Sustainability, Nagoya University,
Furo-cho, Chikusa-ku, Nagoya, Aichi 464-8603, Japan
e-mail: niinomi@imr.tohoku.ac.jp



K. Sasaki et al. (eds.), *Interface Oral Health Science 2016*,
DOI 10.1007/978-981-10-1560-1_1

A novel β-type Ti alloy composed of nontoxic and allergy-free elements (Ti–29Nb–13Ta–4.6Zr mass%, hereafter abbreviated as TNTZ) is a low-Young's modulus Ti alloy developed by Niinomi et al. based on the d-electron design method [1]. This alloy exhibits excellent corrosion resistance and biocompatibility, with a low Young's modulus (~60 GPa), and has thus been investigated for use in many practical applications, including the production of implant rods for spinal fixtures [2]. In spinal fixation rods, the low Young's modulus and excellent biocompatibility of TNTZ is beneficial for patients; however, this alloy possesses only relatively moderate mechanical properties (ultimate tensile strength = ~510 MPa) [1], which are inadequate for practical application. However, according to surgeons specializing in spinal diseases, the implant rod should exhibit a small degree of springback to offer greater handling ability for surgeons, who are required to bend the rod to conform to the curvature of the spine within the limited space inside a patient's body [3]. The amount of springback is determined by both the strength and Young's modulus. Given the same strength, a rod with the higher Young's modulus will exhibit less springback, that is, a high Young's modulus is preferable to suppress springback from the viewpoint of surgeons. There is therefore a conflicting requirement concerning the Young's modulus from the viewpoint of patients and surgeons, which cannot be fully satisfied by TNTZ.

Recently, many researchers [4–7] have focused on the development of new β-type Ti alloys to solve this problem, such as Ti–Mo and Ti–Cr alloys. These alloys possess a novel property called "changeable Young's modulus" or "Young's modulus self-adjustability," in which the deformed region of the material exhibits a high Young's modulus, whereas the Young's modulus of the undeformed region remains low.

Therefore, changeable-Young's modulus Ti alloys suitable for the rods of spinal fixation devices are introduced with a focus on Ti–Mo and Ti–Cr alloys.

## 1.2 Mechanism of Increasing Young's Modulus in Deformed Region

The springback of the deformed rods of spinal fixation device can be reduced by increasing the Young's modulus in the deformed region. This reduction can be achieved if a secondary phase with a high Young's modulus is induced by deformation. In Ti alloys, metastable phases such as α′ martensite with hcp structure, α″ martensite with orthorhombic structure, and ω-phase with hexagonal or trigonal structure can form between the stable α- and β-phases based on the amount of β-stabilizing element, as depicted in the schematic phase diagram of Ti alloys in Fig. 1.1. Therefore, various phases such as α′-, α″-, and ω-phases can be induced by deformation. ω-phase precipitation is known to increase the Young's modulus of the alloys, whereas α′- and α″-phase precipitations result in a decrease. Therefore, if the β-phase stability is controlled for the ω-phase to be induced by deformation, the

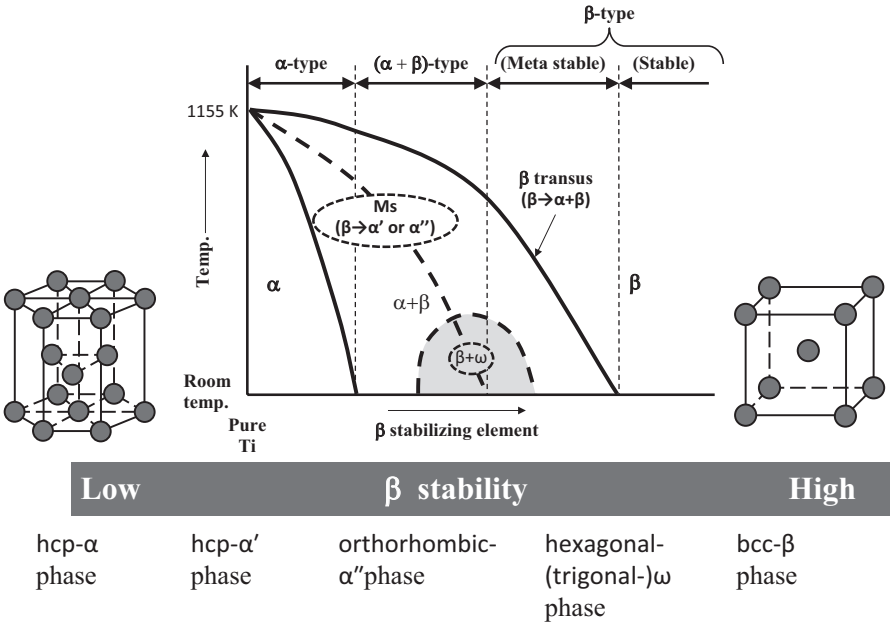


**Fig. 1.1** Relationship between schematic phase diagram of titanium alloys and β stability

Young's modulus of the alloys is partially increased in the deformed region, leading to a decrease in springback of the alloy and thereby maintaining the deformed shape of the rod.

## 1.3 Possible Alloy System

The addition of molybdenum (Mo) results in β-stabilizing properties in Ti alloys [8], and, thus, it is an effective β stabilizer for designing β-type alloys. In addition, Hanada et al. reported that a ω-phase forms during the cold working of as-quenched Ti–Mo alloys within the composition range of 11–18 mass% Mo [9–11]. Thus, it is possible to realize a changeable Young's modulus in metastable Ti–Mo alloys via deformation-induced ω-phase transformation. Moreover, Mo is less toxic than Al and V [1]. Many studies have demonstrated the excellent mechanical compatibility and good cytocompatibility of Ti alloys containing Mo, such as Ti–Mo, Ti–Mo–Ta, and Ti–Mo–Zr–Fe [12–17]. Karthega et al. [18] reported that Ti–15Mo exhibits corrosion resistance similar to that of TNTZ in Hank's solution. Both Zhou et al. and Oliveira et al. [19] reported that Ti–Mo alloys exhibit excellent corrosion resistance.

Hanada et al. reported that the ω-phase forms during the cold working of as-quenched Ti–Cr alloys within the composition range of 8–11.5 mass% Cr [20]. Moreover, the ω-phase can be introduced by deformation at room temperature in

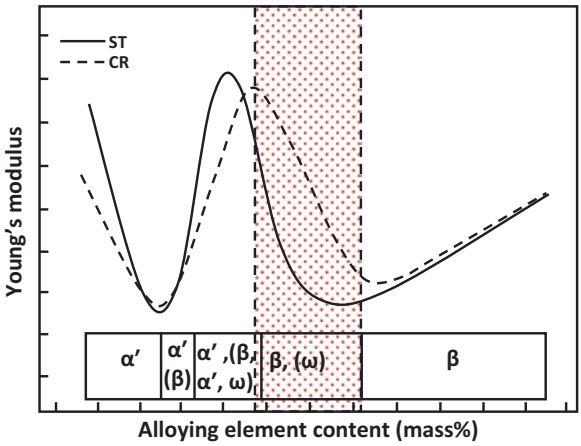


**Fig. 1.2** Schematic variation of Young's modulus in Ti–M (M: β stabilizer) binary alloys as a function of alloying element content. ST and CR indicates solution treatment and cold rolling, respectively

**Table 1.1** Nominal chemical compositions of Ti–Mo and T–Cr systems alloys examined to optimize their chemical compositions exhibiting the greatest increase in Young's modulus after deformation (the best Young's modulus adjustability)

| Ti–Cr system | Ti–10Cr | Ti–11Cr | Ti–12Cr | Ti–13Cr |
|---|---|---|---|---|
| Ti–Mo system | Ti–13Mo | Ti–15Mo | Ti–16Mo | Ti–17Mo |

Ti–V, Ti–Fe, and Ti–Mo metastable β-type alloys [10, 11, 21–23]. Furthermore, Cr is known to control the anodic activity of the alloy and increase the tendency of Ti to passivate [24], and the passive films of Ti alloys, in turn, allow them to maintain corrosion resistance [25–27].

Thus, Mo and Cr are suitable alloying elements to develop Ti-based biomaterials with Young's modulus adjustability.

However, as depicted in the schematic illustration of the relationship between temperature and alloying element content in Fig. 1.2 [23, 28], with each appearing phase, deformation-induced ω-phase precipitation occurs, and the lowest Young's modulus before deformation is highly expected in the relatively high β stability region.

To optimize the chemical compositions of Ti–Mo and Ti–Cr alloys exhibiting the greatest increase in Young's modulus after deformation (the best Young's modulus adjustability), the Mo equivalent, $Mo_{eq}$, was considered, and 1 mass%Cr is equivalent to 1.25 mass%Mo. Then, the Ti–Mo and Ti–Cr alloys, whose nominal chemical compositions are listed in Table 1.1 [29], were examined. The Young's moduli, microstructures, and deformation behaviors of both alloy systems were examined before and after deformation; deformation was simulated by cold rolling with a reduction of 10 %.

## 1.4 Ti–Mo Alloys

### *1.4.1 Microstructures Before and After Deformation*

The X-ray diffraction (XRD) profiles of the Ti–(13–18)Mo alloys subjected to solution treatment and cold rolling with a reduction of 10 % (hereafter called as cold rolling (CR)) are shown in Fig. 1.3 [29, 30]. Only peaks corresponding to the β-phase are detected in each solution-treated (ST) specimen. No peaks corresponding to the ω-phase are detected by XRD. In addition, after cold rolling, only single β-phases are detected in each CR specimen. However, the enlarged XRD profiles of Ti–13Mo alloy subjected to solution treatment (ST) and CR in Fig. 1.4 [29] contain ω- and α″-phase peaks, respectively. For Ti–13Mo alloy, it is apparent that deformation-induced α″-phase transformation occurs.

Figure 1.5 [29, 30] shows selected area electron diffraction patterns of the Ti–(13–18)Mo alloys subjected to ST. The existence of a small amount of athermal ω-phase is recognized in the Ti–(13–16)Mo alloys subjected to ST. As the intensities of the ω reflections decrease with increasing Mo content, the amount of the athermal ω-phase in the ST specimens decreases. It is well known that the amount of the athermal ω-phase in β-type alloys depends on the stability of the β-phase. Specifically, the stability of the β-phase increases with increasing Mo content. Thus, the formation of the athermal ω-phase during water quenching (WQ) is suppressed in high-β-stable alloys. The amount of the athermal ω-phase in Ti–16Mo–ST is thus less than that in Ti–13Mo–ST, and the athermal ω-phase in Ti–17Mo–ST and Ti–18Mo–ST disappears.

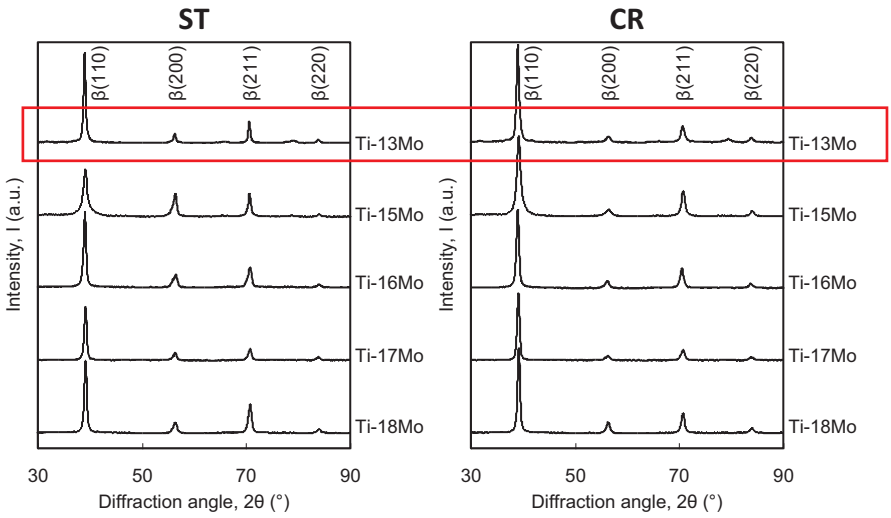


**Fig. 1.3** XRD profiles of Ti–(13–18)Mo alloys subjected to solution treatment (ST) and cold rolling (CR)

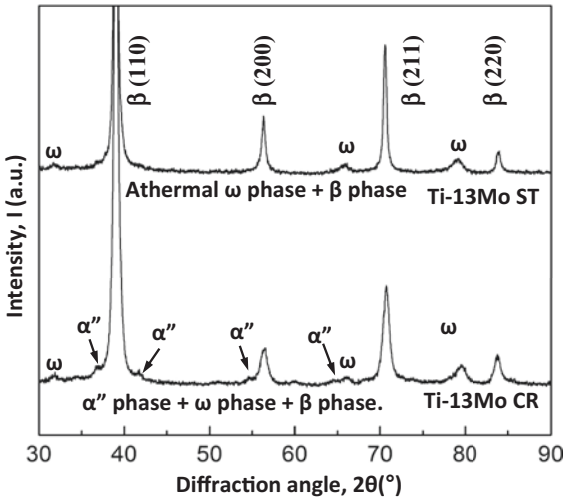


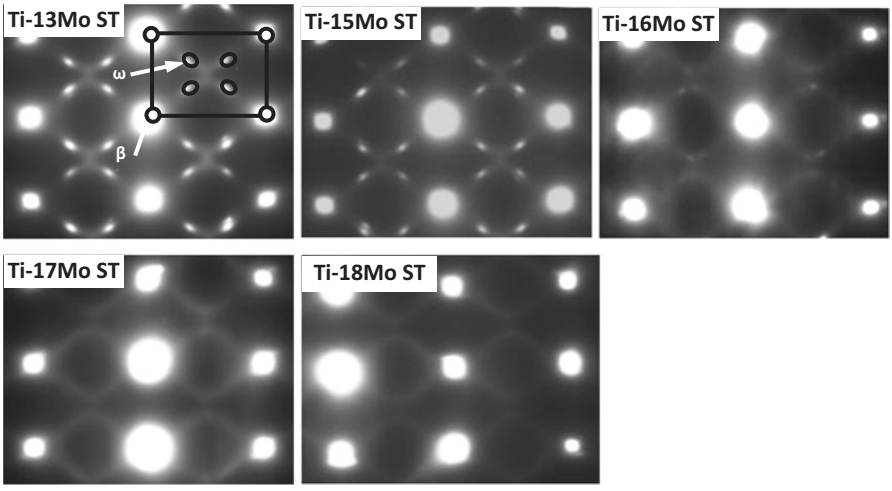


**Fig. 1.4** XRD profiles of Ti–13Mo alloy subjected to solution treatment (ST) and cold rolling (CR)

**Fig. 1.5** Selected area electron diffraction patterns of Ti–(13–18)Mo alloys subjected to solution treatment (ST)

Figure 1.6 [29, 30] shows selected area electron diffraction patterns of the Ti–(13–18)Mo alloys subjected to CR. After cold rolling, the ω spots in all the alloys become sharp. This result confirms that deformation-induced ω-phase transformation occurs during CR. After CR, the ω reflections in Ti–13Mo–Cr, Ti–15Mo–CR, and Ti–16Mo–CR are much sharper than in Ti–13Mo, Ti–15Mo–ST, and Ti–16Mo–ST, indicating that the amount of ω-phase increases because of CR. Moreover, sharp extra spots corresponding to the ω-phase are observed in Ti–17Mo–CR and Ti–18Mo–CR, suggesting that a considerable amount of ω-phase is formed in these two alloys. These findings confirm that deformation-induced ω-phase transforma-

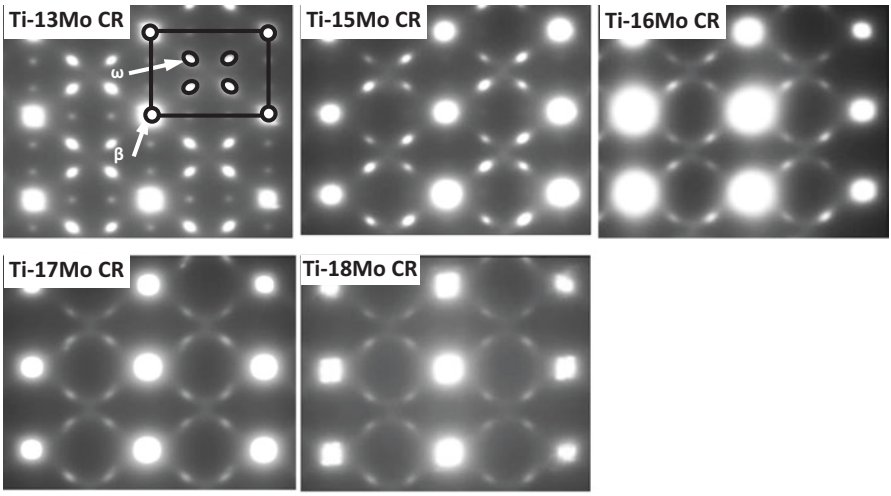


**Fig. 1.6** Selected area electron diffraction patterns of Ti–(13–18)Cr alloys subjected to cold rolling (CR)

tion occurs in all the Ti–(13–18)Mo alloys during CR. With increasing Mo content, the intensities of the ω reflections decrease, indicating that deformation-induced ω-phase transformation is dependent on the stability of the β-phase. Specifically, as the Mo content increases, the stability of the β-phase increases and deformation-induced ω-phase transformation becomes difficult during CR. Thus, the amount of deformation-induced ω-phase decreases with increasing Mo content.

### *1.4.2 Young's Modulus Change by Deformation*

Figure 1.7 [29, 30] shows the Young's moduli of the Ti–(13–18)Mo alloys subjected to solution treatment and CR. Except Ti–13Mo alloy, all the alloys subjected to ST exhibit low Young's moduli of <80 GPa, which is much lower than those of SUS 316 L stainless steel (SUS 316 L), commercially pure titanium (CP Ti), and Ti–6Al–4 V extra low interstitial (ELI) alloy (Ti64 ELI). For the Ti–(15–18)Mo alloys, the Young's moduli of the alloys subjected to CR are higher than those subjected to ST. For the ST specimens, with increasing Mo content, the Young's modulus first decreases slightly from 79 GPa for Ti–15Mo–ST to 73 GPa for Ti–17Mo–ST, after which the value slightly increases to 75 GPa for Ti–18Mo–ST. According to the TEM observation and XRD analysis results, the amount of athermal ω-phase in the alloys decreases with increasing Mo content. There is no athermal ω-phase in Ti–17Mo–ST or Ti–18Mo–ST. The ω-phase is known to have a significant effect on the mechanical properties of Ti alloys and is likely to increase the Young's modulus. In this case, the athermal ω-phase is the main factor contributing to the change in the

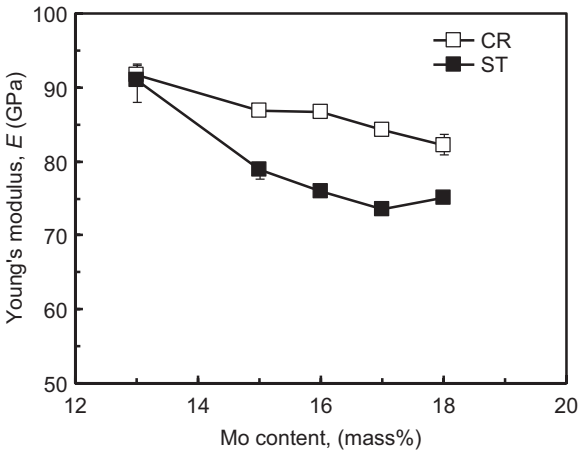


**Fig. 1.7** Young's moduli of Ti–(13–18)Mo alloys subjected to solution treatment (ST) and cold rolling (CR)

Young's modulus. Therefore, the Young's modulus of the alloys first decreases, and Ti–17Mo–ST exhibits the lowest Young's modulus among the designed alloys. With a further increase in the Mo content, the athermal ω-phase in the alloy disappears. Thus, the solid solution strengthening with Mo becomes the primary cause of the changes in the Young's modulus. The Young's modulus increases as the bcc lattice contracts with increasing Mo content. Therefore, the Young's modulus of Ti–18Mo–ST is slightly higher than that of Ti–17Mo–ST. The microstructural analysis indicates that deformation-induced ω-phase transformation occurs in all the alloys. Therefore, the increase in the Young's moduli of these four alloys following CR is attributed to the deformation-induced ω-phase transformation that occurred during CR. The lack of change in the Young's modulus of Ti–13Mo alloy is considered to result from the combined effect of deformation-induced ω-phase transformation and deformation-induced α″-phase transformation.

### *1.4.3 Deformation-Induced Products and Phase Constitutions*

The deformation-induced products in Ti–(13–18)Mo alloys resulting from CR are summarized in Table 1.2 [29]. Except for Ti–13Mo alloy, the ω-phase as well as $\{332\}_\beta<113>_\beta$ and $\{112\}_\beta<111>_\beta$ twins are formed by CR. For Ti–13Mo alloy, the ω- and α″-phase as well as $\{332\}_\beta<113>_\beta$ and $\{112\}_\beta<111>_\beta$ twins are formed by CR.

The constituent phases of the Ti–(13–18)Mo alloys subjected to ST and CR are summarized in Table 1.3 [29]. The constituent phases of the Ti–(13–16)Mo alloys subjected to ST are the β- and athermal ω-phases, whereas that of the Ti–17Mo and Ti–18Mo alloys subjected to ST is ω-phase.

The constituent phases of the Ti–13Mo alloy subjected to CR are β-, athermal ω-, and deformation-induced ω-, and deformation-induced α″-phases. The constituent

**Table 1.2** Summary of deformation-induced products by cold rolling in Ti–Mo alloys

| Alloy | Deformation-induced ω | Deformation-induced α″ | Mechanical twinning ($\{332\}_\beta<113>_\beta$ and $\{112\}_\beta<111>_\beta$) |
|---|---|---|---|
| Ti–13Mo | ☆ | ☆ | ☆ |
| Ti–15Mo | ☆ | × | ☆ |
| Ti–16Mo | ☆ | × | ☆ |
| Ti–17Mo | ☆ | × | ☆ |
| Ti–18Mo | ☆ | × | ☆ |

**Table 1.3** Summary of phase constitutions of Ti–(13–18)Mo alloys subjected to solution treatment (ST) and cold rolling (CR)

| Alloy | Subjected to solution treatment | Subjected to solution treatment and cold rolling |
|---|---|---|
| Ti–13Mo | β + athermal ω | β + athermal ω + deformation-induced ω + deformation-induced α″ |
| Ti–15Mo | β + athermal ω | β + athermal ω + deformation-induced ω |
| Ti–16Mo | β + athermal ω | β + athermal ω + deformation-induced ω |
| Ti–17Mo | β | β + deformation-induced ω |
| Ti–18Mo | β | β + deformation-induced ω |

phases of the Ti–15Mo and Ti–16Mo alloys subjected to CR are the β-, athermal ω-, and deformation-induced ω-phases. Further, the constituent phases of the Ti–16Mo and Ti–17Mo alloys subjected to CR are β- and deformation-induced ω-phases.

### *1.4.4 Springback*

Ti–17Mo alloy exhibited the greatest increase in Young's modulus after CR, as stated above. The ratios of springback per unit load as a function of applied strain for Ti–17Mo alloy, Ti64 ELI, which is the most widely used Ti alloy for biomedical applications, and TNTZ, and strains for the calculation of the springback ratio are shown in Fig. 1.8 [29, 30]. The springback per unit load ratio of Ti–17Mo alloy is smaller than that of TNTZ and close to that of Ti64 ELI and reaches to a stable value for an applied strain greater than 2 %. The springback of a rod composed of Ti–17Mo alloy is expected to be significantly suppressed.

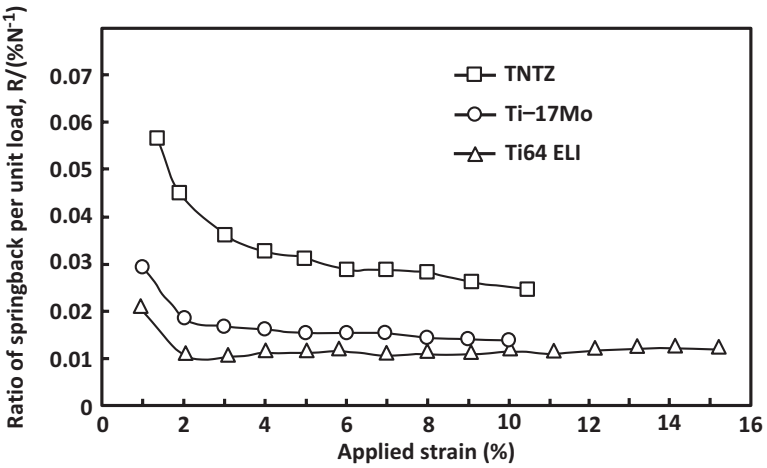


**Fig. 1.8** Ratio of springback per unit load as a function of applied strain for Ti–17Mo alloy, Ti–6Al–4V ELI alloy (Ti64 ELI), and Ti–29Nb–13Ta–4.6Zr alloy (TNTZ) and strains for calculation of the springback ratio

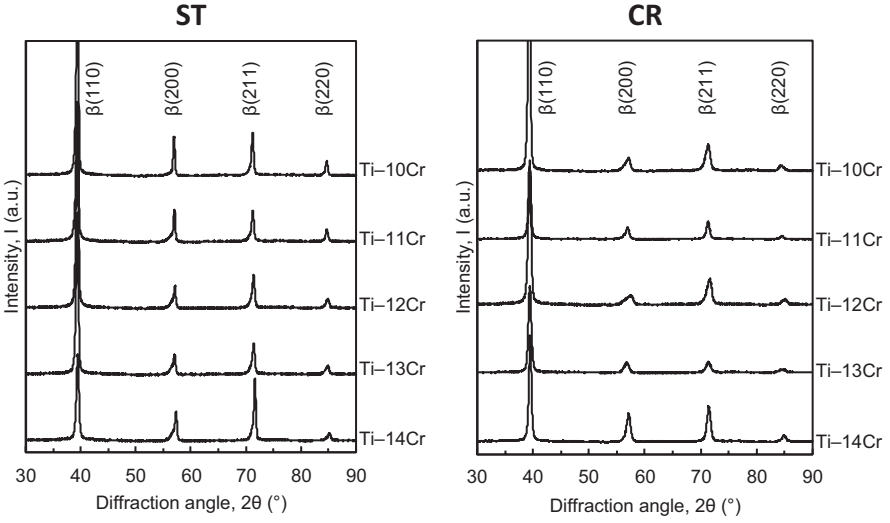


**Fig. 1.9** XRD profiles of Ti–(10–14)Cr alloys subjected to solution treatment (ST) and cold rolling (CR)

## 1.5 Ti–Cr Alloys

### *1.5.1 Microstructures Before and After Deformation*

Figure 1.9 [31] shows the XRD profiles of the Ti–xCr ($x = 10$, 11, 12, 13, and 14 mass%) alloys subjected to ST and CR. Only the peaks corresponding to the bcc β-phase were detected in every specimen under both ST and CR conditions. No peaks corresponding to the ω-phase were detected by XRD.

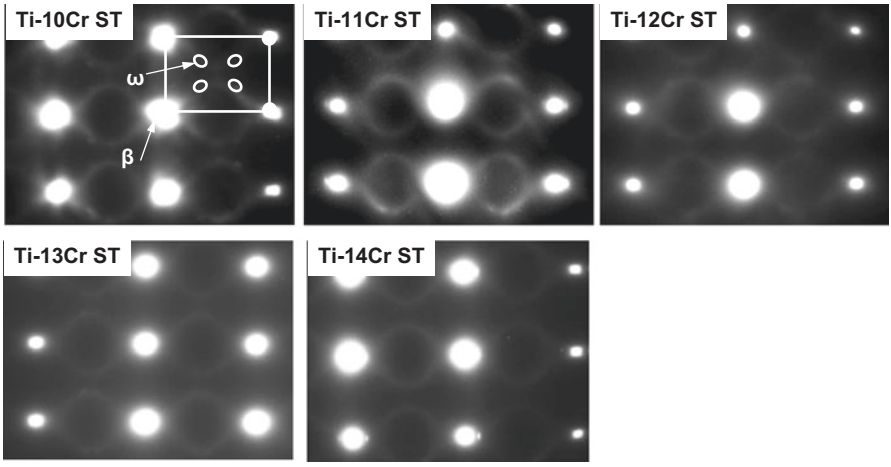


**Fig. 1.10** Selected area electron diffraction patterns of Ti–(10–14)Cr alloys subjected to solution treatment (ST)

Figure 1.10 [31] shows the selected area electron diffraction patterns of the Ti–xCr ($x = 10$, 11, 12, 13, and 14 mass%) alloys subjected to ST. The electron diffraction patterns of the $[110]_\beta$ zone of the Ti–10Cr–ST reveal weak extra spots in addition to spots derived from the β-phase, suggesting that a small amount of the athermal ω-phase is formed in Ti–10Cr–ST during WQ. For Ti–11Cr–ST, the intensities of the ω reflections decrease, which is reflected by the change in the circular diffuse streaks. As observed in Fig. 1.5b–e, as the Cr content continues to increase, the circular diffuse streaks are weakened. It is well known that the intensity of the ω reflection is related to the amount of the ω-phase. The amount of the athermal ω-phase in the designed alloys is observed to be dependent on the stability of the β-phase. Specifically, as the Cr content increased, the β-phase became more stable, leading to suppression of the formation of the athermal ω-phase during water quenching. Therefore, the amount of the athermal ω-phase in Ti–11Cr–ST is lower than that in Ti–10Cr–ST, and the athermal ω-phase disappears almost completely in Ti–12Cr–ST, Ti–13Cr–ST, and Ti–14Cr–ST.

Figure 1.11 [31] shows selected area electron diffraction patterns of the Ti–(1–14)Cr alloys subjected to CR. After CR, the ω reflections in Ti–10Cr–CR are much sharper than in Ti–10Cr–ST, indicating that the amount of the ω-phase increases in response to CR. Furthermore, the intensities of the ω reflections increase in Ti–11Cr–CR and Ti–12Cr–CR compared with those in Ti–11Cr–ST and Ti–12Cr–ST. These findings confirm that the deformation-induced ω-phase transformation occurs in the Ti–10Cr, Ti–11Cr, and Ti–12Cr alloys during CR. The amount of the ω-phase in Ti–10Cr–CR, Ti–11Cr–CR, and Ti–12Cr–CR is too small to be detected by XRD analysis, but the deformation-induced ω-phase is evident upon TEM observation. Specifically, as the Cr content increases, the intensities of the ω reflections

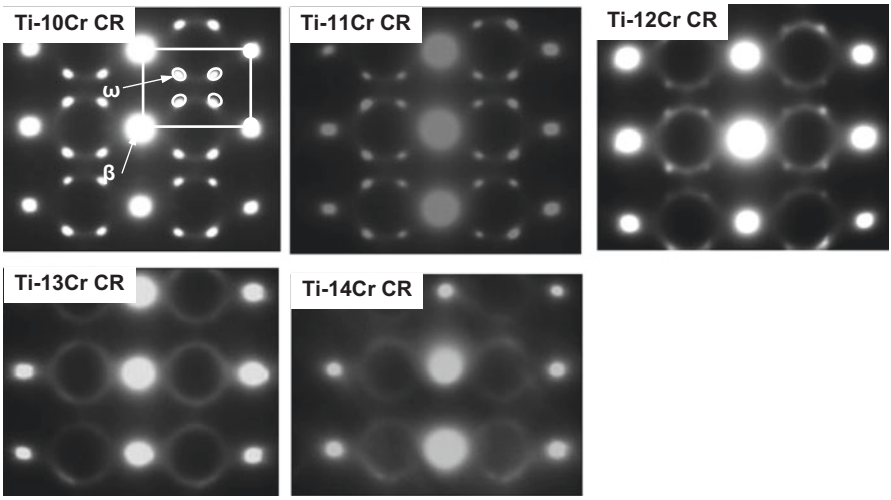


**Fig. 1.11** Selected area electron diffraction patterns of Ti–(10–14)Cr alloys subjected to cold rolling (CR)

decrease. In addition, only diffuse streaks are observed in Ti–13Cr–CR and Ti–14Cr–CR, suggesting that the amount of the ω-phase does not change during cold rolling. These findings indicate that the deformation-induced ω-phase transformation does not occur in Ti–13Cr and Ti–14Cr alloys during CR. Thus, the deformation-induced ω-phase transformation is dependent on the β-phase stability. In lower-stability alloys, such as Ti–10Cr, Ti–11Cr, and Ti–12Cr, the deformation-induced ω-phase transformation may occur; however, with increasing Cr content, the β-phase can become more stable, thereby suppressing the deformation-induced ω-phase transformation. The combined EBSD analysis and TEM observation results indicate that the deformation-induced ω-phase transformation is accompanied by $\{332\}_{\beta}$ mechanical twinning.

### *1.5.2 Young's Modulus Change by Deformation*

Figure 1.12 [31] shows the Young's moduli of the designed alloys subjected to ST and CR. In the ST specimens, as the Cr content increases, the Young's modulus decreases from 82 GPa for Ti–10Cr–ST to 68 GPa for Ti–12Cr–ST and then increases to 79 GPa for Ti–14Cr–ST. The changes in the Young's modulus can be attributed to two primary factors: the athermal ω-phase and solution strength of Cr. When the Cr content is less than 12 mass%, the amount of the athermal ω-phase in the designed alloys decreases drastically as the Cr content increases. In this case, the athermal ω-phase is the main factor responsible for the change in the Young's modulus; therefore, the Young's modulus initially decreases with increasing Cr content. However, when the Cr content increases beyond 12 mass%, the athermal ω-phase is no longer present in the designed alloys; thus, the solid solution strengthening

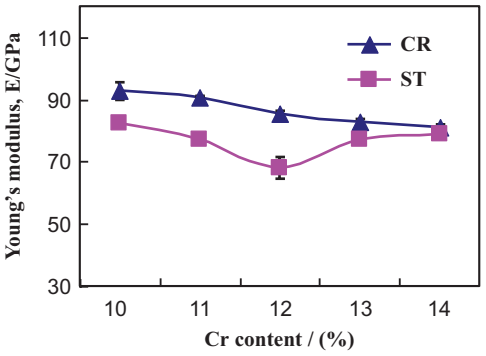


**Fig. 1.12** Young's moduli of Ti–(10–14)Cr alloys subjected to solution treatment (ST) and cold rolling (CR)

becomes the primary cause of the changes in the Young's modulus. As a result, the Young's modulus increases as the Cr content increases from 12 to 14 mass%. After CR, Young's moduli of Ti–10Cr, Ti–11Cr, and Ti–12Cr alloys increase remarkably compared with those after ST, whereas the changes in the moduli of Ti–13Cr and Ti–14Cr are negligible. Microstructural analysis indicates that the deformation-induced ω-phase transformation occurs in Ti–10Cr–CR, Ti–11Cr–CR, and Ti–12Cr–CR and that the ω-phase in β-type Ti alloys is likely to be the source of the increase in the Young's modulus. Therefore, the increase in the Young's moduli observed for these three alloys can be attributed to the deformation-induced ω-phase transformation that occurs during cold rolling. The degree of the increase in the Young's modulus is dependent on the amount of the deformation-induced ω-phase; thus, the Young's moduli of Ti–10Cr–CR, Ti–11Cr–CR, and Ti–12Cr–CR decrease as the Cr content increases. In this study, Ti–12Cr exhibits a low Young's modulus of 68 GPa after ST and a high Young's modulus of 85 GPa after CR.

### *1.5.3 Deformation-Induced Products and Phase Constitutions*

The deformation-induced products formed by CR in the Ti–(10–14)Cr alloys are summarized in Table 1.4 [29]. For the Ti–(11–12)Cr alloys, the deformation-induced ω-phase and $\{332\}_\beta<113>_\beta$ mechanical twins are formed by CR. However, for Ti–13 and Ti–14 alloys, no deformation-induced products are formed by CR.

The constituent phases of the Ti–(10–14)Cr alloys subjected to ST and CR are summarized in Table 1.5 [29]. The constituent phases of the Ti–10 and Ti–11Cr alloys subjected to ST are β- and athermal ω-phases. The constituent phases that of the Ti–(12–14) alloys subjected to ST is the single β-phase.

The constituent phases of the Ti–10Cr and Ti–11Cr alloys subjected to CR are β-, athermal ω-, and deformation-induced ω-phases. The constituent phases of the Ti–12Cr alloy subjected to CR are β- and deformation-induced ω-phases. The constituent phase of the Ti–13Cr and Ti–14Cr alloys subjected to CR is the single β-phase.

**Table 1.4** Summary of deformation-induced products by cold rolling in Ti–Cr alloys

| Alloy | Deformation-induced ω | Deformation-induced α″ | Mechanical twinning ($\{332\}_\beta<113>_\beta$) |
|---|---|---|---|
| Ti–10Cr | ☆ | × | ☆ |
| Ti–11Cr | ☆ | × | ☆ |
| Ti–12Cr | ☆ | × | ☆ |
| Ti–13Cr | × | × | × |
| Ti–14Cr | × | × | × |

**Table 1.5** Summary of phase constitutions of Ti–(1–14)Cr alloys subjected to solution treatment (ST) and cold rolling (CR)

| Alloy | Subjected to solution treatment | Subjected to solution treatment and cold rolling |
|---|---|---|
| Ti–10Cr | β + athermal ω | β + athermal ω + deformation-induced ω |
| Ti–11Cr | β + athermal ω | β + athermal ω + deformation-induced ω |
| Ti–12Cr | β | β + deformation-induced ω |
| Ti–13Cr | β | β |
| Ti–14Cr | β | β |

### *1.5.4 Springback*

Ti–12Cr alloy exhibited the greatest increase in Young's modulus after CR as stated above. The ratios of springback per unit load as a function of applied strain for Ti–12Cr alloy, Ti64 ELI, and TNTZ, and strains for the calculation of the springback ratio are shown in Fig. 1.13 [32]. The springback per unit load ratio of Ti–12Cr alloy is less than that of TNTZ and close to that of Ti64 ELI and reaches to a stable value for an applied strain beyond 2 %. The springback of a rod composed of Ti–13Cr alloy is expected to be significantly suppressed.

## 1.6 Young's Modulus Under Solution Treatment Conditions and Increment Ratio of Young's Modulus by Cold Rolling

To select of the optimal alloy for spinal fixation rods, the relationships between the Young's modulus under ST conditions and increment ratio, IR, of the Young's modulus by CR of Ti–Mo and Ti–Cr alloys are plotted in Fig. 1.14 [29]. IR of the Young's modulus by CR was calculated by the following equation:

$$\mathrm{IR} = \left(E_s - E_c / E_s\right) \times 100\% \tag{1.1}$$

where $E_s$ is the Young's modulus under ST conditions and $E_c$ is the Young's modulus after CR.

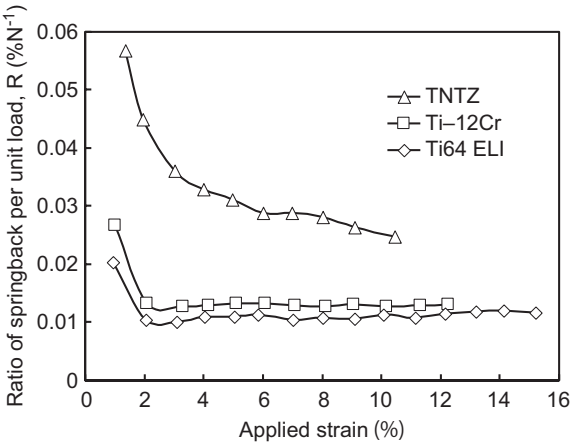


**Fig. 1.13** Ratio of springback per unit load as a function of applied strain for Ti–12Cr alloy, Ti–6Al–4V ELI alloy (Ti64 ELI), and Ti–29Nb–13Ta–4.6Zr alloy (TNTZ) and strains for calculation of the springback ratio

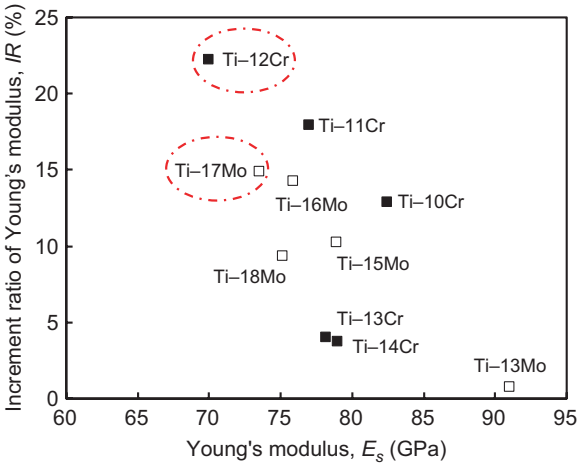


**Fig. 1.14** Distribution of Ti–Cr and Ti–Mo alloys in a plot of Young's modulus under solution-treated (ST) conditions against increment ratio of Young's modulus by cold rolling (CR)

Ti–12Cr alloy exhibits the lowest Young's modulus and highest IR under ST conditions and is thus the most suitable for fixation device rods.

## 1.7 Toward Practical Applications

In the application of Ti alloys with changeable Young's modulus for spinal fixation device rods, their fatigue strengths are highly important. The uniaxial fatigue strength of Ti–12Cr alloy, a Ti alloy with changeable Young's modulus, was examined because it exhibited the lowest Young's modulus and highest IR under ST

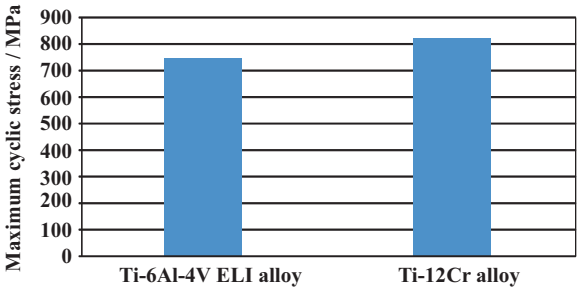


**Fig. 1.15** Fatigue limit of Ti–12Cr alloy and Ti–6Al–4V ELI alloy

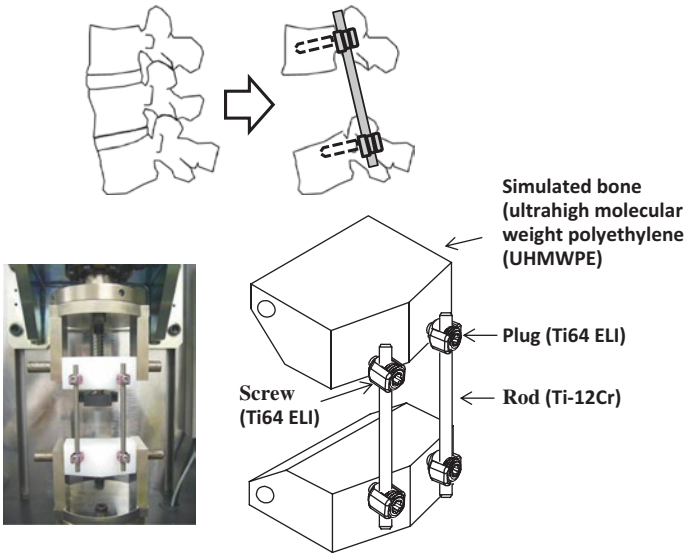


**Fig. 1.16** Schematic drawing of compressive fatigue strength test method according to ASTM F1717

conditions. The results are shown in Fig. 1.15 [33] and demonstrate excellent uniaxial fatigue strength of this alloy. The fatigue limits of Ti–12Cr alloy and Ti64 ELI are shown for comparison. The fatigue ratio, which is the ratio of the fatigue limit to tensile strength, of Ti–12Cr alloy is approximately 0.9, whereas that of Ti64 ELI is approximately 0.6.

However, to employ the alloy in practical rod applications, its endurance must be evaluated in a laboratory according to ASTM F1717, which describes a testing method for evaluating the compressive fatigue strength of spinal fixation rods using a simulated spinal fixation model, as shown in Fig. 1.16 [34]. The spinal fixation device comprises a screw and plug made of Ti64 ELI and a rod made of Ti–12Cr alloy. A Ti64 ELI rod was also used for comparison. Bone was simulated using ultrahigh molecular weight polyethylene (UHMWPE). The compressive fatigue limit of Ti–12Cr alloy subjected to ST is less than that of Ti64 ELI, as shown in

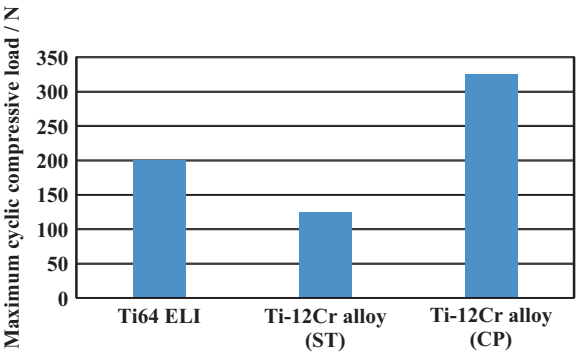


**Fig. 1.17** Compressive fatigue limit of Ti–6Al–4V ELI alloy (Ti64 ELI) and Ti–12Cr alloy subjected to solution treatment (ST) and cavitation peening (CP) after solution treatment evaluated according to ASTM F 1717

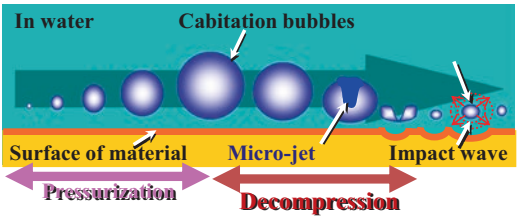


**Fig. 1.18** Schematic drawings of development and crashing of cavitation

Fig. 1.17 [35]. In the ASTM F1717 compressive fatigue test, the rod typically fails at the contact area between the rod and plug. Therefore, fretting that occurs between the rod and plug is thought to reduce the compressive fatigue strength of the rod. An effective solution to such a problem is to improve the mechanical properties and tribological characteristics of the rod. The introduction of a hardened layer via compressive residual stress on the surface of the rod effectively prevents fretting fatigue. Peening techniques can introduce these hardened layers through plastic deformation, i.e., work hardening delivered by a large impact on the material's surface. Among the major peening techniques, cavitation peening, which is schematically illustrated in Fig. 1.18 [36], appears to be a highly promising method for improving the compressive fatigue strength of rods used in spinal fixation devices because it induces less surface damage than other peening techniques. Therefore, cavitation peening was performed on Ti–12Cr alloy rods to improve their compression fatigue strength as evaluated by ASTM F1717; the technique significantly increases the compressive fatigue strength of the rods, as demonstrated in Fig. 1.17.

## 1.8 Summary

Ti–17Mo and Ti–12Cr alloys with changeable Young's modulus are suitable for spinal fixation device rods, but Ti–12Cr alloy is more suitable because of its higher IR of the Young's modulus by deformation and lower Young's modulus. The fatigue strength of Ti–12Cr alloy is high, and its fatigue ratio is approximately 0.9. Ti–12Cr

alloy is highly expected to be used for spinal fixation device rods because its compression fatigue strength, which is evaluated according to the ASTM 17171 standard, is significantly improved by cavitation peening.

**Acknowledgments** This work was partly supported by the interuniversity cooperative research program "Innovative Research for Biosis-Abiosis Intelligent Interface" of the Ministry of Sports, Culture, and Education in Japan and a Grant-in-Aid for Scientific Research (A) and Challenging Exploratory Research from the Japan Society for the Promotion of Science (JSPS).

## References

1. Kuroda D, Niinomi M, Morinaga M, Kato Y, Yashiro T. Design and mechanical properties of new beta type titanium alloys for implant materials. Mater Sci Eng A. 1998;243:244–9.
2. Tamura T, Kozuka S, Oribe K, Nakai M, Niinomi M. Evaluation of Ti-Nb-Ta-Zr as new medical implants. In: Niinomi M, Akiyama S, Hagiwara M, Ikeda M, Maruyama K, editors. Ti-2007 science and technology. Sendai: The Japan Institute of Metals; 2007. p. 1441–4.
3. Steib JP, Dumas R, Skalli W. Surgical correction of scoliosis by in situ contouring – a distortion analysis. Spine. 2004;29:193–9.
4. Nakai M, Niinomi M, Zhao XF, Zhao XL. Self-adjustment of Young's modulus in biomedical titanium alloys during orthopaedic operation. Mater Lett. 2011;65:688–90.
5. Zhao XF, Niinomi M, Nakai M, Hieda J, Ishimoto T, Nakano T. Optimization of Cr content of metastable β-type Ti-Cr alloys with changeable Young's modulus for spinal fixation applications. Acta Biomater. 2012;8:2392–400.
6. Zhao XF, Niinomi M, Nakai M, Hieda J. Beta type Ti-Mo alloys with changeable Young's modulus for spinal fixation applications. Acta Biomater. 2012;8:1990–7.
7. Zhao XL, Niinomi M, Nakai M, Miyamoto G, Furuhara T. Microstructures and mechanical properties of metastable Ti-30Zr-(Cr, Mo) alloys with changeable Young's modulus for spinal fixation applications. Acta Biomater. 2011;7:3230–6.
8. Narushima N. Metallic biomaterials: titanium and its alloys. J Jpn Soc Biomater. 2005;23:86–95.
9. Hanada S, Yoshio T, Izumi O. Effect of plastic deformation modes on tensile properties of beta titanium alloys. Trans Jpn Inst Metals. 1986;27:496–503.
10. Hanada S, Izumi O. Correlation of tensile properties, deformation modes, and phase stability in commercial β phase titanium alloys. Metall Trans A. 1987;18:265–71.
11. Hanada S, Izumi O. Transmission electron microscopic observations of mechanical twinning in metastable beta titanium alloys. Metall Trans A. 1986;17:1409–20.
12. Ho WF, Ju CP, Chern Lin JH. Structure and properties of cast Ti–Mo alloys. Biomater. 1999;20:2115–22.
13. Wang K. The use of titanium for medical applications in the USA. Mater Sci Eng A. 1996;213:134–7.
14. Ho WF. A comparison of tensile properties and corrosion behavior of cast Ti–7.5Mo with c.p. Ti, Ti–15Mo and Ti–6Al–4V alloys. J Alloy Compd. 2008;464:580–3.
15. Lin DJ, Chuang CC, Chern Lin JH, Lee JW, Ju CP, Yin HS. Bone, formation at the surface of low modulus Ti–7.5Mo implants in rabbit femur. Biomater. 2007;28:2582–9.
16. Gordin DM, Gloriant T, Texier G, Thibon I, Ansel D, Duval JL, Nagel MD. Development of a β type Ti–12Mo–5Ta alloy for biomedical applications: cytocompatibility and metallurgical aspects. J Mater Sci Mater Med. 2004;15:885–91.
17. Trentania L, Pelilloa F, Pavesia FC, Ceciliania L, Cettab G, Forlino A. Evaluation of the TiMo12Zr6Fe2 alloy or orthopaedic implants: in vitro biocompatibility study by using primary human fibroblasts and osteoblasts. Biomater. 2002;23:2863–9.
18. Karthega M, Raman V, Rajendran N. Influence of potential on the electrochemical behavior of beta titanium. Acta Biomater. 2007;3:1019–23.

19. Zhou YL, Luo DM. Corrosion behavior of Ti–Mo alloys cold rolled and heat treated. J Alloy Compd. 2011;509:6267–72.
20. Hanad S, Izumi O. Deformation behaviour of retained β phase in β-eutectoid Ti-Cr alloys. J Mater Sci. 1986;21:4131–9.
21. Kuan TS, Ahrens RR, Sass SL. The stress-induced omega phase transformation in Ti-V alloys. Metall Trans A. 1975;6:1767–74.
22. Oka M, Taniguchi Y. {332} Deformation twins in a Ti–15.5 pct V alloy. Metall Trans A. 1979;10:651–3.
23. Matsumoto H, Watanabe H, Masahashi N, Handa S. Composition dependence of Young's modulus in Ti–V, Ti–Nb, and Ti–V–Sn alloys. Metall Trans A. 2006;37:3239–49.
24. Donachie MJ. Titanium: a technical guide. 2nd ed. Materials Park: ASM International; 2000. p. 126.
25. Hanawa T, Ota M. Characterization of surface film formed on titanium in electrolyte using XPS. Appl Surf Sci. 1992;55:269–76.
26. Ong JL, Lucas LC, Raikar GN, Connatser R, Gregory JC. Spectroscopic characterization of passivated titanium in a physiologic solution. J Mater Sci Mater Med. 1995;6:113–9.
27. Hanawa T, Asami K, Asaoka K. Repassivation of titanium and surface oxide film regenerated in simulated bioliquid. J Biomed Mater Res. 1998;40:530–8.
28. Hao YL, Li SJ, Sun SY, Zheng CY, Yang R. Elastic deformation behavior of Ti-24Nb-4Zr-7.9Sn for biomedical applications. Acta Biomater. 2007;3:277–86.
29. Zhao XF. Research and development of binary β-type titanium alloys with changeable Young's modulus for spinal fixation applications. PhD thesis. Tohoku University. (2012).
30. Zhao XF, Niinomi M, Nakai M, Hieda J. Beta-type Ti-Mo alloys with changeable Young's modulus for spinal fixation applications. Acta Biomater. 2012;8:1990–7.
31. Zhao XF, Niinomi M, Nakai M, Hieda J. Optimization of Cr content of metastable β-type Ti-Cr alloys with changeable Young's modulus for spinal fixation applications. Acta Biomater. 2012;8:2392–400.
32. Liu HH, Niinomi M, Nakai M, Hieda J, Cho K. Deformation-induced changeable Young's modulus with high strength in β-type Ti-Cr-O alloys for spinal fixture. J Mech Behav Biomed. 2014;30:205–13.
33. Nakai M, Niinomi M, Liu H et al. Fatigue properties of Ti-12Cr alloy with changeable elastic modulus, collected abstracts of 2015 autumn meeting of the Japan Institute of Metals and Materials. (2015). J21.
34. ASTM F1717-15: standard test methods for spinal implant constructs in a vertebrectomy model, ASTM standard. West Conshohocken, PA, ASTM Int.
35. Narita K, Niinomi M, Nakai M, Suyalatu T et al. Improvement of endurance of β-type titanium alloys by cavitation peening treatment. Collected abstracts of 2014 autumn meeting of the Japan Institute of Metals and Materials. (2014). p. 380.
36. Niinomi M, Li H, Nakai M, Liu H, Liu Y. Biomedical titanium alloys with Young's moduli close to that of cortical bone. Regen Biomater. 2016;3:1–13.